Band-gap states of Ti, V, and Cr in 4*H*-SiC: Identification and characterization by elemental transmutation of radioactive isotopes

Norbert Achtziger* and Wolfgang Witthuhn
Institut für Festkörperphysik, Friedrich-Schiller-Universität Jena, Max Wien Platz 1, D-07743 Jena, Germany
(Received 6 August 1997; revised manuscript received 14 October 1997)

Band-gap states in 4*H*-silicon carbide (SiC) are created by radioactive isotopes and detected by repeated deep-level transient spectroscopy measurements. Band-gap states involving a parent or a daughter isotope are uniquely identified by their decreasing or increasing concentration during the nuclear transmutation. Epitaxial layers of *n*-type 4*H*-SiC are doped with ^{48}V or ^{51}Cr by recoil implantation and annealing at 1600 K. These isotopes decay to ^{48}Ti or ^{51}V with half-lives of 16.0 or 27.7 d, respectively. The stability of daughter atom configurations is probed by annealing after the transmutation and found to be unstable in the case of ^{51}V. Titanium is found to have a slightly split acceptor state (0.13 and 0.17 eV below the conduction-band edge E_C) and the splitting is attributed to the occupation of the two inequivalent lattice sites of 4*H*-SiC. Vanadium has one level only (0.97 eV below E_C) in the range investigated with an indication of splitting. Cr has three levels: two of them closely spaced at $E_C-0.14$ and -0.18 eV are interpreted as a slightly split double acceptor state and one level at $E_C-0.74$ eV as the corresponding single acceptor state of the same configuration. Within errors, all Ti and Cr atoms form the band-gap states described whereas in the case of V a minority of all atoms only contributes to the band-gap state at $E_C-0.97$ eV. This finding is discussed in terms of different structural configurations. [S0163-1829(98)04019-3]

I. INTRODUCTION

Silicon carbide (SiC) is one of the wide-gap semiconductors that attract great interest in current semiconductor research.[1] Silicon carbide is expected to replace traditional semiconductors like Si or GaAs in some specialized areas like high-power or high-frequency devices. Because of its extreme chemical and thermal stability, it is expected to open up new semiconductor applications in rough environments and high-temperature electronics.[2] All of these perspectives are based on excellent material properties that are described in review articles[1,3–5] and a data collection.[6]

Silicon carbide exists in a variety of crystallographically different polytypes. The great majority of crystal growth, materials research and device development focuses on three of them: the only cubic polytype, termed 3*C*, and the two hexagonal modifications 4*H* and 6*H*. All polytypes consist of tetrahedrally coordinated Si and C atoms, but differ in the stacking sequence. As a consequence, on each sublattice (Si or C) several slightly different lattice sites exist (except for 3*C*), two of them in 4*H* and three of them in 6*H*. They are termed quasicubic or quasihexagonal and the subtle difference may have a significant effect on the band-gap states of impurities. This is well known for the shallow donor nitrogen[3] and will play an important role in the present paper as well. Since the polytype 4*H* is the most promising in view of most applications, the present study investigates this polytype. Similar, but less detailed experiments have been done in the 6*H* polytype[7] as well and will be referenced here for comparison.

Semiconductors are generally extremely sensitive to minor traces of impurities that create an energy level in the band gap. Consequently, there is a general interest in revealing the correlation between a certain element or defect and its band-gap states. This knowledge is the necessary basis to either identify impurities in a given material by detecting their band-gap states or to adjust material properties by intentional doping with a certain element. For the transition metals investigated in the present study, both aspects are important.

Several techniques are available to detect and characterize band-gap states in a semiconductor, but most of them do not reveal their origin that may be an intrinsic defect or an impurity. An approach[8–10] to avoid any ambiguity in the chemical assignment of band-gap states has been developed in recent years by applying the radiotracer concept—as well known, e.g., for diffusion studies—to semiconductor spectroscopy. The basic idea is straightforward: a crystal is doped with a radioactive ''parent'' isotope of the element of interest and the spectroscopic measurement is performed repeatedly several times during the elemental transmutation to the ''daughter'' isotope. Band-gap states—or, more generally speaking, any element-specific consequences—of the parent element will be characterized uniquely by a decrease of the concentration that will exactly reflect the nuclear decay, characterized by a known half-life. Similarly, the concentration of daughter element related states will increase.

In the present work, deep-level transient spectroscopy (DLTS) is used to detect and analyze band-gap states in SiC. Analogous experiments have been performed in silicon.[10–12]

There are two main reasons why the transition metals Ti, V, and Cr are of special interest in silicon carbide. (i) They are—except for shallow dopants like B and N—the most frequent residual impurities in SiC crystals.[13,14] There is a discussion whether vanadium is the main reason[15] for the short carrier lifetime typical for SiC or not.[16] (ii) Vanadium has been successfully used as a deep compensating center to produce semi-insulating material (urgently needed for high

TABLE I. List of isotopes and technical parameters of the recoil implantation. Each isotope has been produced alternatively by (p,n) or (α,n) reactions.

Radioactive parent isotope	Half-life (d)	Stable daughter isotope	Nuclear reaction	Primary beam	Target foil, thickness (μm)	Useful target isotope, abundance	Coimplanted stable elements	Isotopic purity of parent
^{48}V	15.97	^{48}Ti	(p,n)	11 MeV p	Ti, 0.29	^{48}Ti, 73.9%	Ti	79 (5) %
^{48}V	15.97	^{48}Ti	(α,n)	16.5 MeV α	Sc, 0.82	^{45}Sc, 100%	Sc,Ti	100%
^{51}Cr	27.7	^{51}V	(p,n)	11 MeV p	V, 0.28	^{51}V, 99.8%	V	100%
^{51}Cr	27.7	^{51}V	(α,n)	16.5 MeV α	Ti, 0.99	^{48}Ti, 73.9%	Ti, V	65 (5) %

frequency devices) both by doping during growth[14] and by ion implantation.[17] The compensation mechanism is closely linked to the deep-level positions of vanadium. Since the compensating effect in originally n-type material is not sufficient at high temperatures, a search for other impurities with suitable deep levels is desirable.

Most of the available information about the transition metals under investigation arises from magnetic resonance experiments[18] and optical transitions. Titanium has been detected by electron spin resonance[19,20] (ESR) and its near-band-gap luminescence is well established,[19,21–23] leading to the proposal of an acceptor state very close to the conduction band that was recently confirmed by DLTS.[24] Vanadium has been identified as an amphoteric center by ESR (Refs. 25 and 26) and near-infrared optical transitions[19,25–31] are known. In contrast to its well-established midgap donor state,[19,27,32] the position of an acceptor level[32–36] is still a matter of discussion. Available information about Cr is comparatively rare and restricted to magnetic resonance[18,26,37] and photoluminescence.[18] Except for our own preceding reports,[38,39] to our knowledge, no information about the position of band-gap states is available.

The present study will clarify the existence and energetic position of band-gap states of these elements, quantify their degree of electrical activation, and discuss the assignment of different levels to atomic configurations. The part of the band gap accessible by our DLTS experiments ranges from about 0.12 to about 1.1 eV below the conduction-band edge[40] and thus leaves two-thirds of the band gap unobserved.

II. EXPERIMENTAL PROCEDURE

The radioactive isotopes used in the present study are ^{48}V and ^{51}Cr. The isotope ^{48}V decays to the stable isotope ^{48}Ti with a half-life of 15.97 d. The second isotope used, ^{51}Cr, decays to stable ^{51}V with a half-life of 27.7 d. The properties of these isotopes and technical parameters of their production are summarized in Table I.

A. Implantation of radioactive isotopes

Both radioactive isotopes were produced and instantaneously implanted into the samples by recoil implantation. The implantations were performed at the tandem accelerator of the University Erlangen-Nürnberg (Germany). The basic procedure is as follows: A primary beam of protons or α particles induces nuclear reactions when passing through a thin target foil. Due to the recoil transferred to the reaction products, these are kicked out of the target foil and implanted into the samples mounted off-axis to the primary beam. The implantation energy is distributed between zero and a maximum energy of about 0.6 or 2.3 MeV in the case of (p,n) or (α,n) nuclear reactions. A sketch of the experimental setup and a general description of this technique can be found in Ref. 41.

In addition to the desired radioisotope, its daughter element is implanted simultaneously with a fluence in the same order of magnitude. Consequently, the concentration of the daughter element is nonzero at the beginning and will then increase during transmutation. For nuclear reactions starting on the polyisotopic Ti foil, there is also a coimplantation of stable isotopes of the parent element (see Table II, isotopic purity). Though the chemical purity of the recoil implantation is far from perfect, there is no better procedure available[10] to perform radioactive doping with V or Cr isotopes.

During implantation, a part of the samples was masked to have an unimplanted reference area on the same sample. The number of radioisotopes implanted into each sample is determined by γ spectroscopy and is given in Table II as an implantation fluence. The γ spectra exclude the presence of other γ-emitting isotopes and thus prove that no other radioactive isotope contributes to the decay-induced change of the sample on the time scale of interest.[42]

B. Sample preparation

All samples were epitaxial CVD (chemical vapor deposition) layers of 4H SiC (thickness 5 μm) on silicon-face, heavily doped 4H-SiC substrates. Layers and substrates were grown by Cree Research Inc. The conductivity was n type and had been adjusted by nitrogen doping. The net donor concentration in the epilayer was in the range of $(3-5)\times10^{15}$ cm^{-3}. Some of the samples were analyzed by Raman spectroscopy to detect polytype specific vibration modes;[43] no indication of a polytype other than 4H was detected. DLTS measurements on as-grown samples revealed one electron trap only with an energy of 0.63 (2) eV and a low concentration of 10^{12} cm^{-3}, indicating a high quality of the epitaxial layer. Since radiotracer experiments require a high sensitivity to additionally incorporated impurities, this is a basic prerequisite for the present experiments.

After implantation, the samples were annealed in sealed quartz ampoules filled with oxygen. For most of the samples (see Table II), the annealing process was at 1600 K for 4 h. After oxide etching in hydrofluoric acid, electrical contacts were produced by thermal evaporation of titanium onto the

TABLE II. List of samples, including data about the recoil implantation and annealing conditions. The activity ratio specifies the fraction of activity remaining in the sample after annealing and oxide etching.

Sample	Nuclear reaction parent isotope	Implanted fluence (10^{10} cm^{-2})	Annealing process	Activity ratio: remaining vs implanted
1	(p,n) ^{51}Cr	7.9	1650 K, 1.5 h, O_2	0.26
2	(p,n) ^{51}Cr	6.4	1600 K, 4 h, O_2	0.21
3	(p,n) ^{51}Cr	2.1	1600 K, 4 h, O_2	0.32
4	(p,n) ^{51}Cr	2.3	1650 K, 3 h, O_2	0.25
5	(p,n) ^{51}Cr	1.6	1650 K, 3 h, O_2	0.25
6	(α,n) ^{51}Cr	3.6	1600 K, 4 h, O_2	0.63
7	(α,n) ^{51}Cr	3.0	1600 K, 4 h, O_2	0.63
8	(α,n) ^{51}Cr	2.5	1600 K, 4 h, O_2	0.63
9	(α,n) ^{51}Cr	3.6	1600 K, 4 h, O_2	0.58
10	(p,n) ^{51}Cr	3.1	1600 K, 4 h, Ar + 1600 K, 0.6 h, O_2	0.60
11	(p,n) ^{51}Cr	2.9	1600 K, 4 h, Ar + 1600 K 0.6 h, O_2	0.57
12	(p,n) ^{48}V	0.5	1600 K, 4 h, O_2	0.34
13	(p,n) ^{48}V	0.7	1650 K, 3 h, O_2	0.24
14	(p,n) ^{48}V	0.8	1600 K, 4 h, O_2	0.23
15	(α,n) ^{48}V	1.6	1600 K, 4 h, O_2	0.80
16	(α,n) ^{48}V	2.6	1600 K, 4 h, O_2	0.65
17	(α,n) ^{48}V	1.8	1600 K, 4 h, O_2	0.65

substrate and of aluminum (dots with typically 0.5 mm diameter) onto the partly implanted epitaxial layer. Finally, the samples were heated in argon atmosphere at 800 K for 5 min.

The oxidizing annealing process was chosen to avoid surface decomposition[44] and to ensure a high-quality surface for the subsequent preparation of Schottky contacts. The depth of the oxide layer was measured by a mechanical step profiler to be 0.14 (4) μm. Oxide formation and etching is the main reason for the considerable loss of implanted radioisotopes of up to 80% in samples doped by (p,n) reaction. An initial anneal in argon and subsequent oxidation clearly reduces this loss (samples 10 and 11). For (α,n)-implanted samples, the loss is smaller because of the higher implantation energy (Table II).

The annealing process is taken as the time zero of the delay time during transmutation, because it is this process that establishes both the depth distribution and the structural configuration of the implanted isotopes. Later on, this initial state is not subject to any intentional modification except for the elemental transmutation.

Some implanted samples were analyzed by admittance spectroscopy,[45,46] clearly revealing the two ionization levels of the shallow nitrogen donors.[47,48] No other peaks in the admittance spectra exist, i.e., the shallow doping of the samples is exclusively due to nitrogen and no influence of the radiotracer implantation is detectable by admittance spectroscopy.

C. Deep-level transient spectroscopy

Detailed explanations of the technique may be found in the literature.[49–51] The spectra were recorded by a commercial DLTS system.[52] During one temperature scan with a rate of typically 0.05 K/s, capacitance transients with several different measuring parameters and the capacitance-voltage (CV) characteristics of the Schottky contact were measured. Unless otherwise stated, all spectra shown are taken with a reverse bias voltage $U_R = -2$ V, a pulse voltage $U_P = 0$ V, a pulse length of 1 ms, and a predefined time window of 100 ms. To obtain depth profiles or the field strength dependence, the capacitance transients were evaluated individually according to the Fourier technique described by Weiss and Kassing[53] to obtain amplitude and time constant τ directly. To obtain classical DLTS spectra, the correlation between the transient and various weighting functions was calculated. In all figures shown, one period of the sine function was used. Clearly, this DLTS signal may be regarded as the first Fourier sine coefficient of the transient, labeled b_1. By normalization, the height of a DLTS peak equals the amplitude of the exponential capacitance transient. The trap parameters energy E_T and capture cross section σ (assumed to be independent of temperature) were derived as usual[50,51,54] from an Arrhenius plot of $\ln(T^2\tau)$ covering three orders of magnitude of the time constant τ (1 ms to 1 s). If one would alternatively assume[55] $\sigma(T) \propto T^{-n}$ with $n=2$ or $n=3$, the resulting trap energies would be greater by $+nkT$ (T is the mean DLTS peak temperature and k the Boltzmann constant). The errors given for the trap energy include only those errors influencing the slope of the Arrhenius plot, but not systematic uncertainties[50] of DLTS.

D. Relevance of decay-induced defects

The basic idea of radiotracer spectroscopy was already described in the introduction. In contrast to results obtained

for the parent isotope which are always characteristic for the specific element, the interpretation of daughter-related features may be more complicated for the following reasons. (i) The nuclear decay results in an excited atomic shell, especially in the case of an electron capture decay, and might thus induce nonequilibrium chemical reactions of the daughter atom. (ii) A nuclear decay generally imposes a recoil onto the daughter atom by emitting radiation quanta. If the recoil energy is high enough, it may either produce intrinsic defects by kicking out neighboring host atoms and the daughter atom may be displaced or be involved in complexes with such defects.[56]

These mechanisms and the resulting configurations will be collectively referred to as ''decay-induced defects.'' As an additional complication, the lattice site or bonding configuration of the parent isotope may be an unstable position for the daughter element, or a site that is not occupied by the daughter element if it is incorporated directly by doping or as a residual impurity.

To judge the relevance of the decay-induced recoil, the recoil energy of the daughter isotopes will now be calculated. The dominating decay path of ^{48}V involves an electron capture (EC) decay or a β^+ decay with equal probabilities and two subsequent γ emissions.[57,58] Since the mean lifetime of the intermediate states is long[58] (>1 ps) compared to the time required to hit a neighboring atom (recoil of the preceding decay), the individual emissions have to be treated separately. The maximum recoil is either 33 eV due to the neutrino of the EC decay or 19 eV due to the first γ quantum in the case of the β^+ decay. The decay of ^{51}Cr mainly proceeds by EC decay to the ground state[57,58] of ^{51}V, resulting in a monoenergetic recoil of 6 eV due to the emitted neutrino. In preceding publications,[7,10,38,39] a wrong value of this recoil energy had been given, resulting in misleading implications on recoil-induced defects.

The recoil energy is to be compared to the displacement energy of SiC. Barry *et al.*[59] derive a displacement energy of 21.8 eV from electron irradiation experiments. Molecular-dynamics calculations[60] yield individual threshold energies for each site and each knock-on direction with the lowest value of 25 eV for carbon displacement along the [111] axis in $3C$-SiC. These lower limits of the displacement energy are similar to the recoil of the ^{48}Ti daughter isotope, i.e., decay-induced effects might be possible for this isotope, at least for a fraction of the transmuting atoms. In the case of the ^{51}V daughter atom, a recoil-induced effect is not expected. This argumentation, however, is a crude estimate only since the displacement energy refers to the pure crystal whereas an impurity may act differently. A comparison to silicon may be of interest here: no indication for decay-induced defects is found for both radioisotopes in similar radiotracer-DLTS experiments in Si, though the displacement energy of Si is significantly smaller (13 eV).[11,41]

III. IDENTIFICATION OF BAND-GAP STATES BY ELEMENTAL TRANSMUTATION

This section presents the DLTS spectra measured during the elemental transmutation and derives the chemical identification of the band-gap states. After complete transmutation, the stability of the daughter atom's configuration is probed by additional post-transmutation annealing.

A. Transmutation experiments and results

All samples were annealed within a few days after implantation and measured by DLTS several times during the transmutation. Figure 1 presents DLTS spectra of samples 2, 6, 12, and 15, i.e., one example for each radioisotope (^{51}Cr or ^{48}V) and way of production [nuclear reaction (p,n) or (α,n), see Table II]. In these spectra, only the initial, the ''final'' (delay time: at least four half-lives) and a reference spectrum from an unimplanted part of the sample are shown. In all spectra, peaks with a time-dependent height exist. They are labeled by numbers from 1 to 6. Their peak height is plotted versus delay time in the right column of Fig. 1. In addition, there are peaks that stay constant in time, labeled $A-D$. The trap energy E_T and capture cross section σ of each level are given in Table III and illustrated in Fig. 2.

After ^{51}Cr implantation in sample 2 [Fig. 1(a)], the four peaks dominating the spectrum are changing with delay time. Two slightly separated peaks labeled 1 and 2 at low temperatures are decreasing. Their peak position and their trap parameters stay constant during this decrease. Finally, two tiny peaks with lower peak temperatures remain (most probably due to a Ti contamination). Because of these underlying peaks, the peak height of level 1 versus delay time as shown in Fig. 1(b) has an apparent offset. The largest peak (3) in the initial spectrum decreases as well whereas its trap parameters remain constant. A peak labeled 4 is present from the very beginning and then increases during delay time without any change in its trap parameters. Two additional peaks in the spectra, labeled B and C, do not change. Except for the absolute peak heights, the same observations as described and shown for this sample are also made for the samples 3 (Ref. 61) and 5.

After implanting the same radioisotope by the (α,n) nuclear reaction (sample 6), the sequentially measured spectra [Fig. 1(c)] again reveal the peaks 1, 2, and 3 and an exponential decrease of their peak height. Around 415 K, the spectra slightly increase with delay time by 6 fF only. This tiny effect is too small to create a defined peak. In comparison to the samples discussed before, there is no clear indication of peak 4 with similar intensity.

The same behavior, i.e., dominating peaks 1, 2, and 3, no peak 4 and a small increase only at about 420 K, is observed as well in the samples 1, 4, 7, 8, and 9. This list demonstrates that the absence of level 4 is not restricted to samples implanted by (α,n) nuclear reaction. Additional ^{51}Cr implanted samples will be discussed in the context of post-transmutation annealing experiments in Sec. III C.

Samples implanted with ^{48}V also reveal time-dependent DLTS spectra as shown for sample 12 implanted via (p,n) reaction in Fig. 1(e). Two peaks labeled 5 and 6 below 100 K are present from the very beginning and increase with delay time. A peak at 430 K decreases exponentially. Its trap parameters are identical to peak 4 in ^{51}Cr-implanted samples (Fig. 2).

Peaks remaining constant in time are present as well $(A-D)$. There is no obvious correlation to the kind or fluence of the implanted atoms. Note the different scales within Fig. 1: peaks $A-D$ appear to be large in Fig. 1(e) only be-

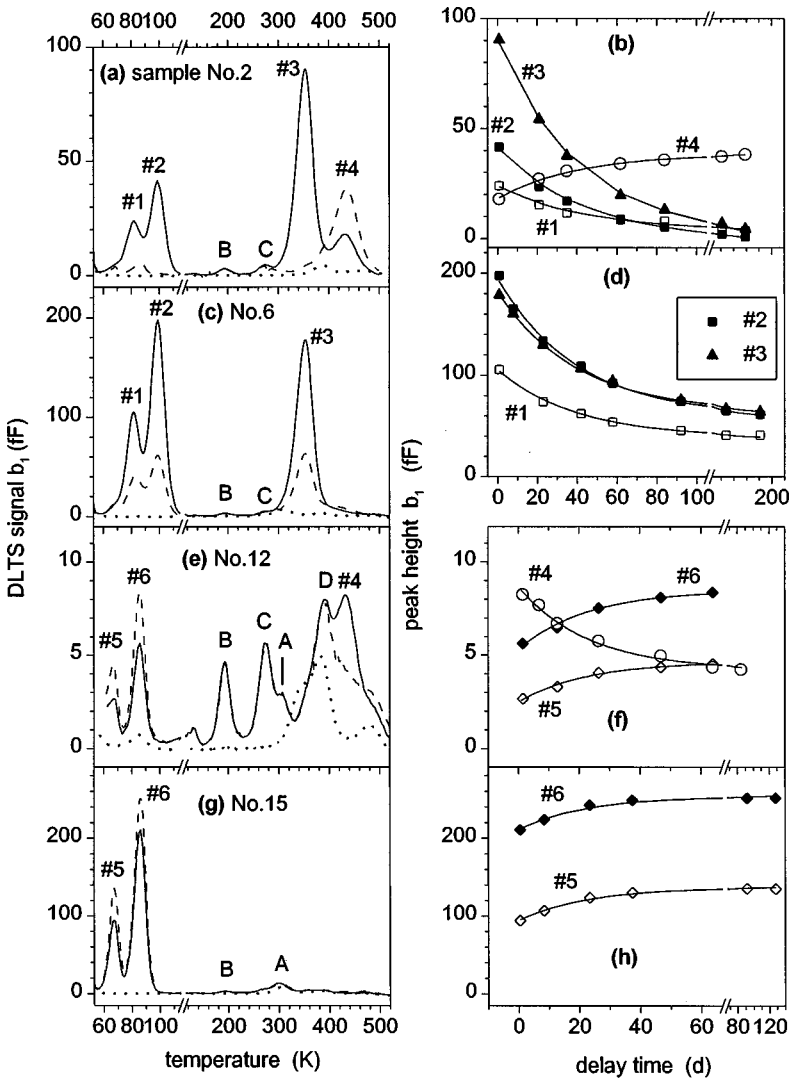

FIG. 1. DLTS spectra of four *n*-type 4*H*-SiC samples doped with radioactive ^{51}Cr (a),(c) or ^{48}V (e),(g). The solid lines display the initial measurement (within 2 d after annealing), the dashed lines display the ''final'' spectrum after a long delay time (at least four half-lives), and the dotted line is a reference spectrum of an unimplanted part of the sample. The height of peaks 1–6 vs delay time is shown in the right column. The solid lines in these figures are a fit of an exponential function with the half-life of the nuclear decay fixed (27.7 d for ^{51}Cr, and 16 d for ^{48}V).

cause of the small peak height changes and the resulting scale of the plot. These peaks remain perfectly stable during delay time: the dashed line of the finally measured spectrum is completely hidden by the initial spectrum. This impressively demonstrates the reproducibility of the DLTS spectra.

Peaks 5 and 6 are present initially and then increase during the observation time in all ^{48}V-implanted samples. For the (α,n) implanted sample 15, this is demonstrated in Fig. 1(g). However, peak 4 is missing. The spectra of another (α,n) implanted sample, 16, are shown in Fig. 3(a). In this case, a small peak at 420 K decreases; within errors, it is compatible with level 4. This peak height change, however, is smaller than the corresponding increase of levels 5 and 6 by a factor of 20. To illustrate the changes more clearly, Fig. 3(b) also shows the difference of measured spectra (initial spectrum subtracted). A measurement with larger reverse bias, i.e., with a sensitive region deeper in the sample, reveals qualitatively the same peak height changes [Fig. 3(c)].

All peaks presented were analyzed by variation of the filling pulse length in a range from 5 μs to 100 ms. No indication of a partial trap filling was found. This result establishes a lower limit for the capture cross section of 2×10^{-18} cm^{-2}. This limit is compatible with the capture cross sections determined from the Arrhenius plot (Table III).

The transmutation experiments may be summarized as follows:in all ^{51}Cr-implanted samples, there are three peaks 1, 2, and 3 that decrease exponentially with delay time. Levels 5 and 6 are present initially in all ^{48}V implanted samples and then increase with delay time. Level 4 exists in a part of the samples only. If present, it clearly increases in ^{51}Cr-doped samples and decreases in ^{48}V-doped samples.

B. Discussion of level identification

The height of all time-dependent peaks discussed above is shown as a function of the delay time in the right column of Fig. 1. For all samples shown, the capacitances in the whole temperature range do not change with delay time and consequently the peak height is strictly proportional to the concentration of the corresponding band-gap state. Since the reproducibility of the spectra is excellent (<1 fF), the DLTS peak heights are determined accurately. The calculation of a trap concentration, however, involves additional sources of error as discussed below. Therefore it is reasonable to discuss the transmutation effects in terms of the peak height instead of concentration.

The peak height versus delay time data were fitted by exponentially decreasing or increasing functions of the type $c_1\exp(-\lambda t)+c_2$ or $c_1[1-\exp(-\lambda t)]+c_2$, respectively, with

TABLE III. Energy E_T and capture cross section σ (assumed to be independent of temperature) of band-gap states n-type 4H-SiC. (a) lists parameters of the Ti, V, and Cr levels and (b) lists further levels that are not correlated with these elements. The half-lives described the peak height vs delay time dependence of the DLTS spectra. The parameter n quantifies the influence of the electric-field strength on the electron emission rate of the trap.

(a)

Level	1	2	3	4	5	6
E_T (eV)	0.143 (10)	0.178 (10)	0.741 (15)	0.970 (30)[a]	0.127 (9)	0.170 (9)
σ (10^{-15} cm^2)	1.2	0.8	2	8	6	10
$T_{1/2}$ (^{51}Cr implant)	27.4 (3.4)	26.9 (2.5)	28.1 (3.9)	23.3 (3.4)		
$T_{1/2}$ (^{48}V implant)				15.8 (3.8)	14.6 (3.0)	16.0 (3.8)
Field dependence n	0.21 (6)	0.22 (6)	<0.05	<0.1	0.16 (5)	0.13 (5)
Chemical identification	Cr	Cr	Cr	V	Ti	Ti
Interpretation	1-/2-	1-/2-	0/1-	0/1-	0/1-	0/1-
(charge, site)	hex.	cub.	both	both	hex.	cub.

(b)

Level	*A*	*B*	*C*	*D*
E_T (eV)	0.640 (25)	0.414 (17)	0.578 (13)	0.855 (25)
σ (10^{-15} cm^2)	2.5	10	4	7

[a]The anomalous DLTS peak width may be interpreted as a level splitting by 0.04 eV, see Ref. 39.

free fit parameters c_1 and c_2. The decay constant λ is linked to the half-life $T_{1/2}$ via $\lambda = \ln 2/T_{1/2}$. The solid curves shown in the right column of Fig. 1 are fits with the half-life fixed to the nuclear half-life of the isotope used. The good agreement with the experimental data is immediately obvious. Alternatively, the half-life may be treated as an additional free fit parameter. The resulting values are given in part (a) of Table III with error limits including all samples. The deviation of the individual fit results from the expected nuclear half-life are small (typically $<10\%$) for peaks 1, 2, and 3 because these peaks undergo strong peak height effects. For the peaks 4, 5, and 6, the fit results scatter by typically 20%.

Peaks 1, 2, and 3 are decreasing exponentially in perfect agreement with the nuclear half-life of ^{51}Cr. This observation definitely proves that each of these levels is created by a defect that is either identical to exactly one[62,63] Cr atom or which contains one Cr atom, eventually with other constituents. These Cr related levels vanish completely in samples doped via (p,n) reaction, whereas a constant offset of 35% of the initial peak height remains in all samples doped by (α,n) reaction. This offset is due to stable Cr isotopes and thus reveals the degree of isotopic purity (Table I) of the ^{51}Cr implantation via (α,n) reaction.

The height of peak 4 also exhibits an exponential time dependence in good agreement with the nuclear half-life. This is a definite proof that level 4 is due to a defect containing exactly one V atom. Obviously, the same level of V is detected both with decreasing concentration if V is the parent atom [Fig. 1(f)] and with increasing concentration if V is the daughter of the ^{51}Cr decay [Fig. 1(b)]. In all samples with an increasing peak 4, the peak is present from the very beginning. This is reasonable for a V related peak, because stable V isotopes are coimplanted together with the radioisotope ^{51}Cr.

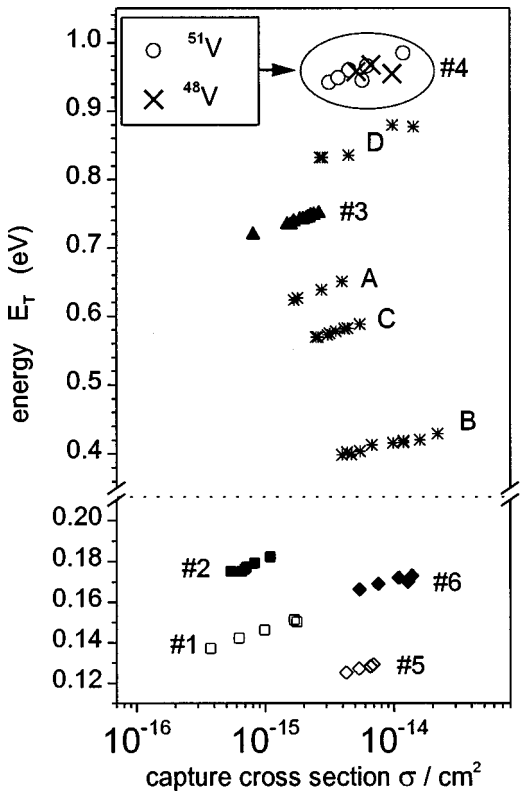

FIG. 2. Graphic representation of the activation energy E_T vs capture cross section σ for all band-gap states detected. Each group of data points represents one band-gap state; the different points within one group reflect different samples. In the case of level 4, the circles are from ^{51}Cr implanted samples (decay to ^{51}V), where peak 4 is increasing during transmutation; the crosses are from ^{48}V-doped samples where it is decreasing.

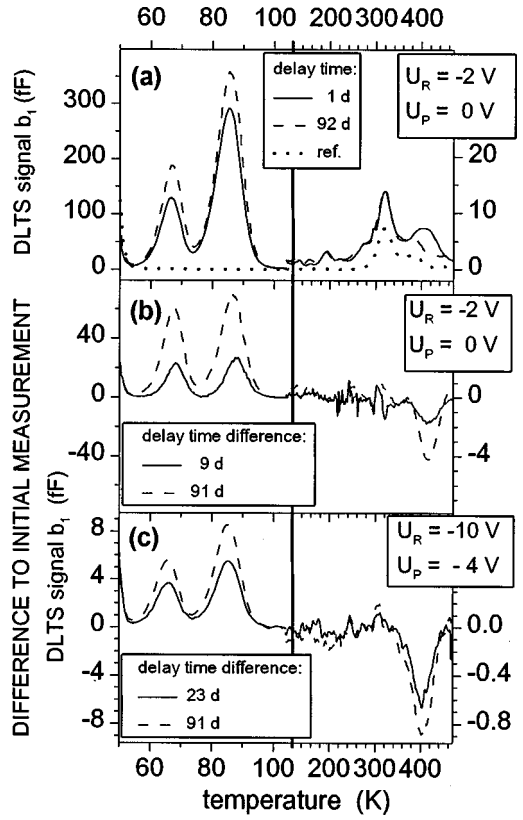

FIG. 3. DLTS spectra of the ^{48}V-doped sample 16. The right part of each spectrum is enlarged by a factor of 10. (a) DLTS spectra under standard measuring conditions, including an initial measurement after 1 d, a measurement after complete transmutation to ^{48}Ti, and a reference spectrum. (b) Difference of spectra relative to the initial spectrum. Same sample and conditions as in (a). (c) Difference spectra of the same sample, measured with greater reverse bias and pulse voltages.

In several ^{51}Cr-implanted samples, a well-defined peak 4 is missing. Instead, a small increase of the DLTS signal with delay time is observed around 420 K [Figs. 1(c), 4(a), and 4(c)]. The attempt to interpreted it as the growth of an additional peak results in a rather uncertain trap energy between 0.82 and 0.96 eV. It can neither be excluded nor proven that these tiny effects in the DLTS spectra are due to an additional V-correlated level with slightly smaller energy than level 4. In the following, this uncertainty will be ignored and these DLTS signals will be interpreted as level 4. In any case, the uncertainty described concerns at most 8% of the vanadium atoms. It has to be stressed that the bad reproducibility of the existence of level 4 does not impair the identification of this level with vanadium: whenever the level is present, its concentration follows the elemental transmutation.

In contrast to all other peaks, peak 4 is broader than expected for a single level as it is illustrated in Fig. 3 of Ref. 39. The peak width can be explained by a superposition of two peaks with equal concentrations and capture cross sections and an energy difference of 0.04 eV.[39] However, there might be as well a difference in the capture cross sections leading to different value for the level splitting. Since the splitting is not really resolved, we continue to refer to peak 4 as one level in the following text.

Levels 5 and 6 are observed with increasing concentration only. In principle, these levels might be due to decay-induced defects. However, both levels are present from the very beginning as it is expected for Ti atoms because of the coimplantation of stable Ti isotopes during the recoil implantation. This finding, however, could not be explained by decay-induced defects, because such configurations should grow during transmutation only, i.e., start from zero. This means[64] that the formation of levels 5 and 6 does not involve decay-induced defects. Instead, they represent the equilibrium configuration of a Ti atom SiC.

C. Post-transmutation annealing experiments

The following group of experiments was performed to clarify whether the daughter element configurations originating from the elemental transmutation are stable equilibrium states. Several samples were annealed after a long delay time of at least five half-lives, i.e., after practically complete transmutation to the daughter element. Up to 850 K, the annealing steps were performed without removing the electrical contacts from the samples.

DLTS spectra of these experiments on ^{51}Cr-implanted samples are shown in Fig. 4. To enable a comparison of the peak height with the initial state of the sample, both the initial spectrum (a few days after ^{51}Cr implantation), the ''final'' spectrum (completely transmuted), and a spectrum after annealing at 800 K for 5 min in argon are shown. Since annealing above 750 K frequently changes the barrier height and thus the capacitance of the contacts (by at most 10%), the spectra shown are normalized to the capacitance to compensate for this effect. In the spectra of samples 4 and 9 [Figs. 4(a) and 4(c)], where the transmutation alone has not been creating peak 4, this peak clearly shows up after 800 K annealing. Its trap parameters are identical to those observed in the transmutation experiments. In sample 5, where peak 4 is detectable already after transmutation, it grows further due to annealing [Fig. 4(b)]. In sample 9 [Fig. 4(c)], the Cr levels are still present after complete transmutation because of stable Cr isotopes. They remain unaffected by annealing. The decrease of the DLTS signal around 350 K visible in Figs. 4(a) and 4(b) is probably due to an annealing effect at some other, unidentified level, since these samples do not contain Cr any more at the time of annealing. The increase of peak 4 was detected in all ^{51}Cr-implanted samples subject to this post-transmutation annealing at temperatures around 800 K. The onset of this annealing effect was at 750 K. Significantly higher annealing temperatures, however, reduce the height of peak 4, as it is shown in Fig. 4(c) for a 1400-K anneal. The Cr peak 3 again remains unaffected.[65]

In the case of ^{48}V-implanted samples, post-transmutation annealing at 800 K does not affect the spectra.

A second kind of experiment was performed with two identically prepared, ^{51}Cr-implanted samples. After each delay time interval during the elemental transmutation, at first one spectrum was taken in the ''as-transmuted state,'' then an annealing step at 800 K in argon for 5 min was performed, and then one more spectrum was taken in the ''annealed state.'' This procedure was repeated after each additional delay (sample 10). The control sample (11) was measured at the same delay times, but without annealing

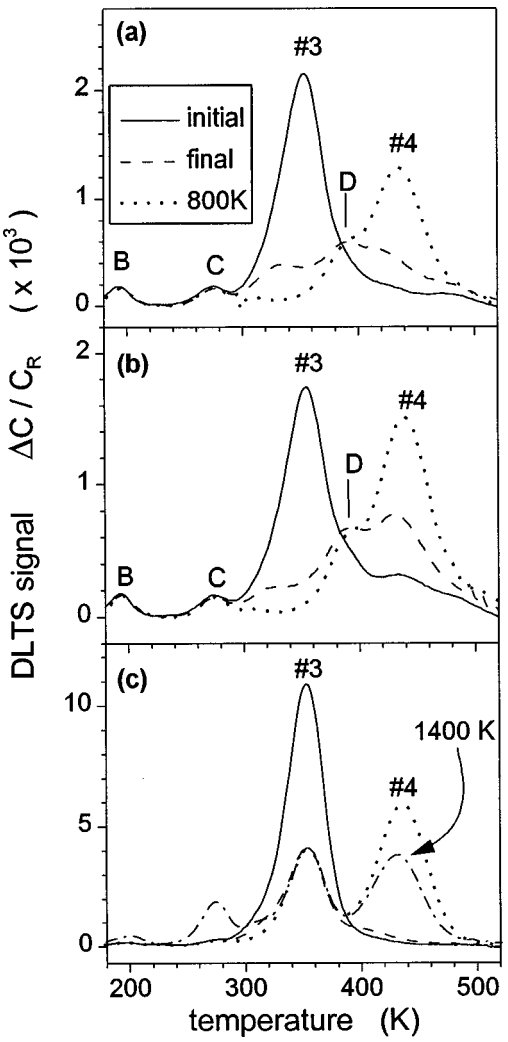

FIG. 4. DLTS spectra of three ^{51}Cr implanted samples (a)–(c), (4, 5, and 9) measured initially (solid line), after complete transmutation to ^{51}V (dashed line) and after a subsequent annealing step at 800 K for 5 min (dotted line). For sample 9 (c), an additional spectrum after annealing at 1400 K is shown (dotted-dashed line).

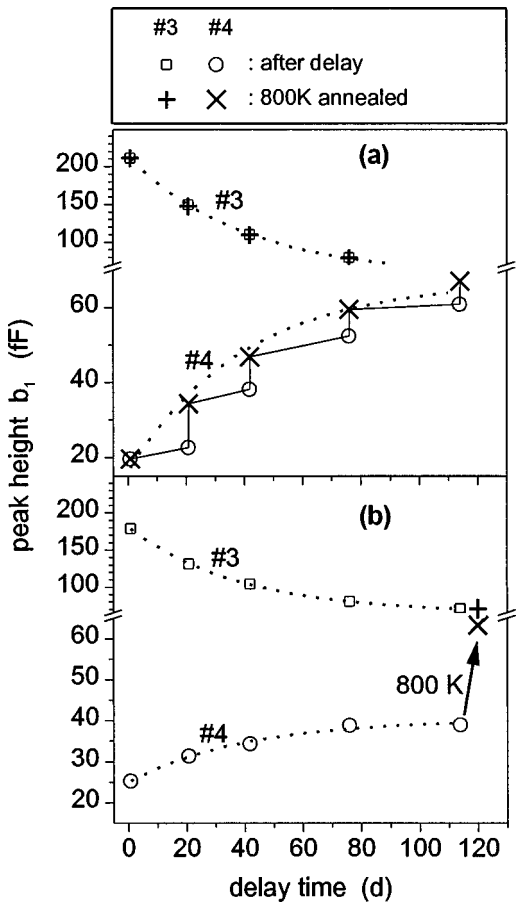

FIG. 5. Peak heights of peak 3 and 4 of samples 10 (a) and 11 (b) during delay time. Open symbols reflect measurements performed after storage at room temperature; crosses reflect measurements directly after 800 K annealing. The solid curve connects subsequently measured data points. The dotted lines are exponential fits with fixed half-life. The final data point of peak 3 is omitted in (a) to avoid overlap with data from peak 4. Note that the peak height axis is broken to show the annealing effect of level 4 more clearly; the total change of peak 3 is larger by a factor of 3 compared to level 4.

prior to individual measurements. One annealing step only was performed at the end of the observation time. The peak heights of levels 3 and 4 during this experiment are shown in Fig. 5 and reveal the following results: the Cr peak 3 is completely unaffected by the annealing (as well as the peaks 1 and 2, not shown). Peak 4 increases by a small amount only during the individual delay time intervals. Each annealing step, however, increases the peak height markedly. For sample 10, this results in a steplike peak height during the sample's history. For the control sample, the increase due to decay at room temperature alone is comparatively small until the final annealing step raises peak 4 to the same height as in the sequentially annealed case.

The post-transmutation experiments may be summarized as follows: Neither Cr nor Ti related levels are sensitive to annealing in the temperature range discussed. A large fraction or even all of the ^{51}V daughter atoms do not contribute to the formation of level 4 during room-temperature storage. After additional annealing, at least a part of them contributes to level 4. This happens in all samples examined, whether level 4 is present before annealing or not.

IV. PROPERTIES OF Ti, V, AND Cr BAND-GAP STATES

In this section, the depth profiles of the traps and the influence of the electric-field strength will be presented. The degree of electrical activation will be quantified and a comparison to the literature will be made.

A. Depth profiles

Depth profiles were routinely obtained for all traps showing a well-defined DLTS peak. They are a necessary prerequisite for the quantitative evaluation of the trap concentration.

The depth profiles of the Cr related levels 1, 2, and 3 in sample 2 are compared in Fig. 6(a). The profile shapes are the same, the absolute concentration of levels 1 and 2 are identical and about one half of the concentration of level 3. The accessible depth range for profiling the low-temperature peaks, however, is small. Therefore, we shall use level 3 to discuss the profile of chromium. In Fig. 6(b), the profile of level 3 of this sample [implanted by (p,n) reaction] is com-

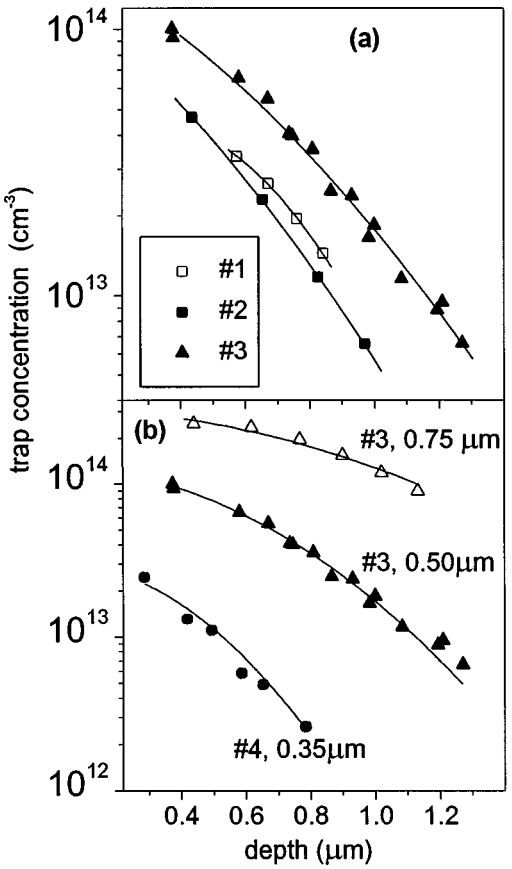

FIG. 6. Concentration profiles of Cr and V related levels measured isothermally by variation of pulse and reverse bias voltages. (a) Initial depth profile of the three Cr levels 1, 2, and 3 in sample 2. The lines are a guide to the eye only. (b) Initial depth profiles of the Cr level 3 in a (p,n)-implanted sample (2, filled triangles) and in an (α,n)-implanted sample (6, open triangles). Initial depth profiles of the V level 4 in sample 2 (filled circles). The solid lines are fits of a Gaussian profile centered at the surface. The resulting width s (standard deviation) is given for each profile.

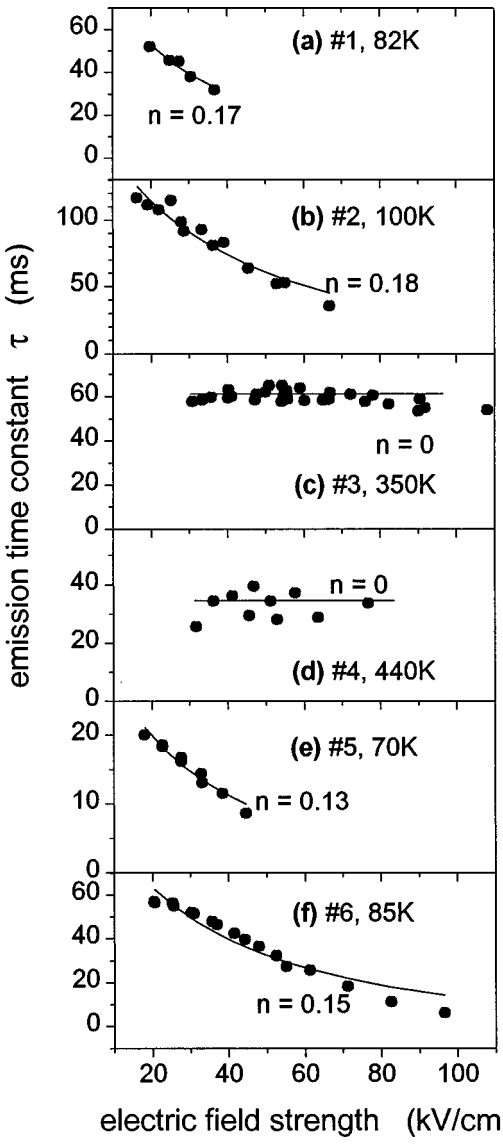

FIG. 7. Dependence of the emission time constant of levels 1–6 (a)–(f) on the electric-field strength at constant temperature. The solid lines are a fit of the Poole-Frenkel effect to the data, treating the charge number n of the center as a free parameter. The resulting values are to be understood as a formal measure only.

pared to the profile of sample 6 implanted via (α,n) nuclear reaction. Both profile shapes are well reproduced by a Gaussian curve centered at the surface. The profile widths (standard deviation) are $s=0.5\,\mu$m and $s=0.75\,\mu$m for the (p,n)- and (α,n)-implanted samples, respectively.

The vanadium depth profiles cannot be obtained from the small peak 4 in ^{48}V-implanted samples [Figs. 1(e) and 3(a)]. For (p,n) implantation, however, a typical vanadium profile is obtained from the initial peak 4 in ^{51}Cr-doped samples [Fig. 1(a)], which is due to co-implanted stable V isotopes. Because of the similar implantation energy, this profile is representative for the profile of ^{48}V in ^{48}Ti(p,n) ^{48}V-implanted samples. It is slightly shallower than the Cr profiles (width $s=0.35\,\mu$m).

The measured depth profiles may be influenced both by implantation and diffusion during annealing. Though the initial implantation profiles are not known precisely, a safe upper limit for the diffusion constant D is derived by equating the smallest profile width to the diffusion length $(2Dt_a)^{1/2}$, where t_a is the annealing time. The resulting upper limit is 10^{-13} cm^2/s for Ti, V, and Cr at 1600 K.

B. Influence of the electric-field strength

The emission time constant of a trap is the primarily measured quantity of DLTS. Because of the strong electric field within the space charge region of the diode, it may be reduced compared to zero-field conditions. For a Coulomb-attractive trap in a uniform electric field and a thermally activated transition over the resulting barrier (Poole-Frenkel effect), the effect has been calculated by Hartke.[66] It depends on the absolute charge number n of the trap after emission and on the electric-field strength. For a neutral trap or a repulsive trap, n is zero and no influence is expected.

To give a quantitative description of the measured data (Fig. 7), they are fitted by this theoretical function, treating the charge number n and the idealized zero-field time constant as free fit parameters. The resulting values of n are given in Fig. 7 (for the data shown) and in Table III (averaged over several samples). It is to be stressed, that this

usage of n is an attempt only to describe the magnitude of the field-strength effect quantitatively. Any fractional number of n does not have a meaning in terms of a fractional charge state. A value close to $n=1$ indicates that the trap is a donor whereas a value close to zero indicates acceptor states.

An influence of the electric-field strength on the emission time constant exist for the levels 1, 2, 5, and 6. The dependence is small compared to the Poole-Frenkel effect of a donor as demonstrated by the small fit results for the parameter n. The deeper levels, 3 and 4, are completely insensitive to the electric field. Though the accessible range of field strength is rather small, especially for levels 1 and 5, the fit results for n are significantly smaller than unity and close to zero. This is a clear indication that all levels are acceptors.

C. Relation between different levels of Ti and Cr

In the case of Ti and V, more than one level is identified. The question arises as to whether these levels are due to different atomic configurations or whether they are different charge states of the same configuration. To answer this question, the concentration ratio of these levels is essential.

As it is obvious from Figs. 1(a) and 1(c) the peak heights of the Cr levels 1, 2, and 3 are neither identical nor exhibit a constant ratio in different samples. Though the peak height of each peak (i.e., at fixed temperature) is strictly proportional to the trap concentration, this is not valid if peaks at different temperatures in the DLTS spectrum are to be compared, for the following reasons: (i) with decreasing temperature, the region that is probed by DLTS moves deeper into the sample; (ii) below 90 K, the shallow doping of the samples starts to freeze out partially; (iii) for the most shallow levels 1 and 5, the energy difference between the donor levels of nitrogen is no longer negligible compared to the level energy.

The concentration of each level is determined according to the Appendix, thus correcting the influence of point (i) only. The resulting concentration ratios are compatible with a 1:1:2 ratio of the Cr levels 1, 2, and 3 and a ratio of 1:1 for the Ti levels 5 and 6. However, the errors of this determination are about 50%, i.e., it is not possible to rigorously prove a specific model by these data (this would require a definite decision between ratios of 1:1 and 1:2). A concentration ratio of about 1:1:2 for the Cr levels 1, 2, and 3 can also be obtained from the depth profiles in Fig. 6(a).

In addition to the concentration ratio, the following considerations are relevant. There are two inequivalent lattice sites on each sublattice in 4H-SiC. In the case of nitrogen[3] and phosphorus,[67] the energy of the corresponding shallow donor states differs by about 50 meV. Since the levels 1, 2, 5, and 6 are close to the conduction band as well, a similar splitting may be expected. Furthermore, both the Ti as well as all Cr related levels appear together in all spectra without any exception that might be expected if any of them would be due to a different lattice site or due to a defect complex. Based on these arguments, the following relation between the observed band gap states is proposed.

The observed Cr levels represent two charge transitions of the same structural Cr configuration: one transition is sensitive to the difference between inequivalent quasicubic or quasihexagonal sites and, therefore, has two slightly different levels 1 and 2. The second transition corresponds to the deep level 3; its energy is insensitive[68] to the tiny difference between inequivalent sites. Levels 5 and 6 are assigned to one configuration of Ti with two inequivalent sites.

D. Degree of electrical activation

The concentration of band-gap states determined by DLTS will now be compared to the number of radioactive atoms in the sample. The fraction of impurity atoms having a band-gap state in the observed part of the band gap is calculated by the following procedure.

(i) Since the width of the depth distribution and the depth probed by DLTS are similar, it is useful to specify the depth-integrated concentration, i.e., the number of traps per surface area N_a. This quantity is determined (for details, see the Appendix) from the total change of the peak height during the transmutation, i.e., band-gap states due to stable isotopes are not included.

(ii) To convert the number of levels (per area) N_a to a number of electrically active isotopes (per area) N_e, the relation between the different levels is essential. Because of freeze-out effects at low temperatures, the data from level 3 are considered to be more accurate than the sum of levels 1 and 2, i.e., $N_e(\mathrm{Cr})=N_a(3)$ is used. In the case of Ti, $N_e(\mathrm{Ti})=2N_a(6)$ is used instead of $N_e(\mathrm{Ti})=N_a(5)+N_a(6)$ for the same reasons. This procedure implicitly assumes an equal population of both inequivalent sites.

(iii) The number of radioisotopes determined by γ spectroscopy of the completely prepared sample is converted into a density (number per area) by taking into account the inhomogeneity of the implantation. The degree of electrical activation is the ratio of N_e to this density.

The results are shown in Fig. 8 for each of the elements and all samples. For vanadium, data are available both for the daughter isotope ^{51}V created by transmutation of ^{51}Cr (to the left of the dashed vertical line) and for directly implanted and annealed ^{48}V. The electrical activation achieved by post-transmutation annealing of ^{51}V daughter atoms is included as well.

In the case of Cr and Ti, the electrical activation is complete and well reproducible; with a few exceptions only, the error bars in Fig. 8 include the case of 100% activation. The complete activation of Ti is especially remarkable because these Ti atoms are formed by the decay of ^{48}V, which behaves in a totally different manner. Within errors, it is possible that the electrically active Ti atoms originate from those V atoms that do not form level 4.

The electrical activation of V is generally low and strongly varies between different samples. The highest activation is achieved by post-transmutation annealing of ^{51}V daughter atoms. Implantation of ^{48}V isotopes followed by annealing leads to a fractional activation of at most 40% in the case of two samples and to a practically vanishing activation below 5% in the other samples. Consequently, vanadium is involved mainly in configurations that do not have a level in the part of the band gap investigated.

E. Summary and comparison to literature

The present section will combine all information derived above and available from the literature. Before discussing the

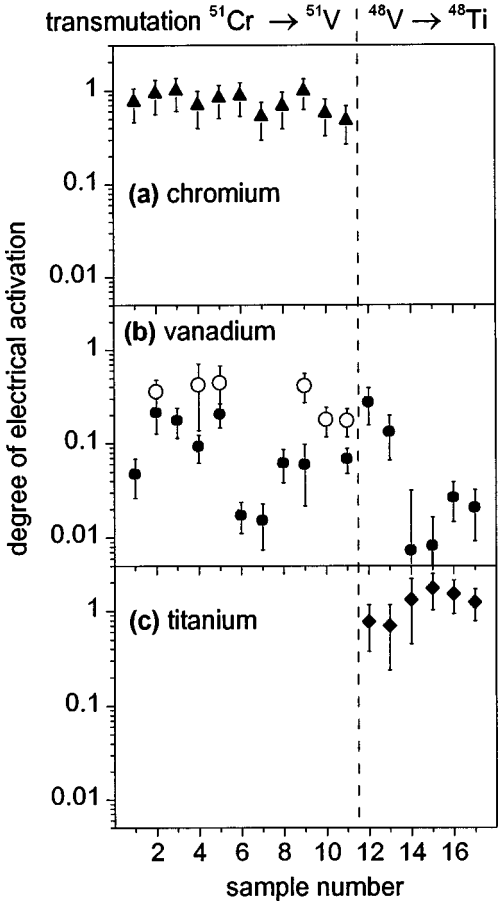

FIG. 8. Degree of electrical activation of Ti, V, and Cr for all samples investigated. The elemental transmutation is indicated on top of the figure. In the case of vanadium, the values obtained after additional post-transmutation annealing are included as open symbols.

individual elements, a short comparison to the results[7] obtained in the polytype 6*H* is given. In 6*H*-SiC, one Cr level at $E_C-0.54$ eV and two slightly separated V levels at $E_C-0.71$ and -0.75 eV are identified. The latter are interpreted to reflect quasicubic and quasihexagonal sites because of their characteristic concentration ratio of 2:1. Following the rule of Langer and Heinrich[69] that deep states may serve as a common reference level in different semiconductors, the similarity between the levels in 4*H* and 6*H* is consistently explained[70] by a band offset of 0.22 (6) eV between both polytypes (E_C lower in 6*H*).

The high and well-reproducible electrical activation of Ti and Cr is a hint that the configuration observed is an isolated atom instead of a defect complex. The formation of such complexes might be expected to depend on variations of implantation fluence or damage. This interpretation is strongly supported by ESR experiments[18] that do not reveal any complex formation at V or Cr atoms. A TiN pair, however, is known,[18] but not of relevance here, since the Ti states observed are formed by transmutation of V atoms. Subsequent pairing with N during room temperature storage can be excluded because of the low concentration and mobility of N. Nevertheless, we have to stress that the involvement of one Ti, V, or Cr atom in the observed defects is definite whereas the exclusion of further constituents in the case of Cr and Ti is an interpretation.

We shall now discuss the individual elements in 4*H*-SiC.

a. Titanium. The two levels 5 and 6 are due to a Ti acceptor state with two energy levels because of the two inequivalent lattice sites available in 4*H*-SiC. This results agrees well with the prediction derived from ESR.[20] The same two DLTS peaks have recently been reported from Ti-implanted 4*H*-SiC by Dalibor *et al.*,[24] assigning the deeper level (6) to the quasicubic site. Practically all Ti atoms originating from the ^{48}V decay create this state which is as well formed by direct implantation of Ti.

b. Chromium. The three levels identified are interpreted as two charge states of one Cr atom occupying the slightly inequivalent quasihexagonal or quasicubic sites. The upper state is sensitive to this difference and is thus split into two levels (1 and 2) whereas the deep state (3) is not. By analogy to titanium, level 2 is proposed to reflect the quasicubic site. Because of the weak or missing field strength effect, the deep level is interpreted as a single acceptor and the state close to the conduction band as a double acceptor. The fraction of Cr atoms creating these levels is high and well reproducible.

There are no level data of chromium available in the literature to compare with. ESR work on Cr-doped 6*H* epilayers has revealed the Cr^{3+} ($3d^3$) and the Cr^{2+} ($3d^4$) state.[18,26,37,71] On a silicon site, these charge states correspond to an acceptor in its singly and doubly ionized state, respectively. This result nicely corresponds[18] to the interpretation of the band-gap states to be an acceptor (3) and a double acceptor (1 and 2). To explain the ESR observation of Cr^{2+} in 6*H*, at least the lower of the Cr double acceptor levels (analogous to 2 of 4*H*) has to be within the band gap of 6*H*-SiC. The rule of Langer and Heinrich,[69] which may be used to compare band-gap states in different polytypes, has been established for really deep levels and may fail if one tries to argue whether a certain state is, say, 50 meV above or below a band edge. Therefore the postulated existence of a Cr double acceptor state in the band gap of 6*H* (analogous to 2 in 4*H*) is not in contradiction to its energy in 4*H* (0.18 eV) and available values for the band offset [0.14 (Ref. 32), 0.25 (Ref. 72), or 0.22 eV (Ref. 70)]. Remarkably, in contrast to the three inequivalent sites detected by ESR for Cr^{3+}, only one quasicubic site[18] has been detected for Cr^{2+}. This finding is naturally explained here, since the upper Cr level 1 (quasihexagonal site) might still be in or very close to the conduction band of 6*H* whereas the deeper level may be close to the nitrogen levels and therefore be occupied in case of low compensation. All together, the present experiments are well compatible with ESR results.

As an alternative explanation, one might increase the charge numbers of the detected band-gap states by one, i.e., interpret levels 1 and 2 as a triple and 3 as a double acceptor transition. This assignment would instantaneously explain a stable Cr^{2+} configuration in *n*-type 6*H*-SiC, but cannot explain the coexistence of Cr^{2+} and Cr^{3+} observed by ESR in heavily *n*-doped SiC.[73] Furthermore, the levels 1 and 2 would be a strongly repulsive center for electrons and a small capture cross sections would be expected, but is not observed. Therefore, this alternative explanation is unlikely.

c. Vanadium. Level 4 at $E_C-0.97(3)$ eV is due to a defect containing exactly one vanadium atom. Based on the DLTS peak broadening, a splitting into two levels with a separation of about 0.04 eV is proposed. The argument used

in the case of Ti and Cr to interpret the defect as a single V atom instead of a defect complex does not hold here, because this state is neither populated by a high fraction of V atoms nor is this fraction reproducible.

The trap energy of level 4 is significantly higher than the value of 0.80 eV obtained by Jenny *et al.*[35] from the resistance of V-compensated SiC. The authors neglect a possible temperature dependence of the mobility μ. This may lead to a systematic deviation that can be estimated as follows: when fitting a Boltzmann factor to temperature dependent data (conductivity), the introduction of an additional preexponential factor $\mu \propto T^{-n}$ will lead to an increase of the resulting activation energy by approximately nkT, where T is the mean temperature of the temperature interval observed. For the data shown by Jenny *et al.* (Fig. 2. of Ref. 35), a value of $n=3$ is required to remove the discrepancy between their value of 0.80 eV and the present DLTS result. This is a reasonable exponent for the mobility versus temperature dependence, i.e., the discrepancy indeed has methodical reasons. Therefore, level 4 is likely to be identical to the level responsible for the compensation of *n*-type SiC.

At first sight, this level 4 seems to fit very well to the expectation of an acceptor state of vanadium residing on the substitutional silicon site (V_{Si}).[19] The majority of vanadium atoms, however, exists in a different configuration which has to be a well-defined site as well since the elemental transmutation of these V atoms creates electrically active Ti daughter atoms. A discussion about this fact and a comparison to further level data from the literature will be given in the next section.

To check whether a low degree of electrical activation is typical for level 4 of vanadium, some data are available in the literature. From the successful compensation of SiC by implantation of V done by Kimoto *et al.*,[17] a degree of electrical activation of at least 20% can be estimated. This number corresponds to the highest value observed by vanadium implantation in the present work. A low degree of electrical activation is reported from Jenny *et al.*,[35] but in this case the vanadium concentration is at least three orders of magnitude higher than in the present work, i.e., the solubility may be of importance. Uddin, Mitsuhashi, and Uemoto[13] detect a level at $E_C-0.72$ eV in 4*H*-SiC that—in contrast to their proposal—is probably identical to level 3 of the present work, i.e., due to Cr. In their bulk crystal, the concentration of vanadium is higher by a factor 7 than that of chromium. Though the DLTS spectra shown do not fully cover the temperature range of the V peak 4, it is obvious that there is no peak 4 with a height exceeding the height of the Cr peak. This is a direct evidence for a low fraction of V atoms forming level 4.

V. DISCUSSION OF LATTICE SITES AND TRANSMUTATION PATHS

In this section, the transmutation paths between the band-gap states and the atomic defect structure will be discussed. We would like to stress that this discussion does not influence the results concerning electrical properties obtained in the sections before. It is an attempt to fully exploit the radiotracer concept even though the analysis technique DLTS itself provides no information about structure.

As it is obvious from the small fraction of observable vanadium (level 4), a consistent explanation requires us to postulate ''nonobserved'' (by DLTS in *n*-type SiC) configurations that do not have a level in the part of the band gap investigated. For the moment, these configurations will be formally labeled by an index to the element's symbol and the relation to real structures will be discussed later on. The slight difference between quasihexagonal or quasicubic lattice sites is ignored here, i.e., the term ''one configuration'' is intended to mean, e.g., all Si-substitutional sites or a specific impurity-defect complex.

There are at least three different configurations of vanadium necessary to explain the present results: (i) a configuration V_{impl} that is mainly populated by implantation and annealing of V, (ii) a configuration V_4 responsible for the observed deep level (4) at $E_C-0.97$ eV, and (iii) a configuration $V_{daughter}$ which is formed by a part of the ^{51}V daughter isotopes and which, in contrast to V_{impl}, transforms to V_4 during annealing at 800 K.

Now, an attempt will be made to correlate those configurations with real defect structures. From ESR experiments,[18] the Si-substitutional site is predicted for all of the three elements; the band-gap states determined in the present work are well compatible with the charges states observed in those experiments as discussed in Sec. IV E. However, two aspects should be kept in mind when comparing DLTS and ESR data: the present DLTS experiments cover only $\frac{1}{3}$ of the band gap, i.e., further band-gap states may exist for a given configuration. On the other hand, there is no information from ESR on the fraction of impurity atoms involved in the configuration observed; i.e., the results are not necessarily characteristic for all impurity atoms.

Because of the high fraction of Cr and Ti atoms occupying one specific configuration, we assume that this observed configuration is identical to the site reported from ESR work, i.e., a silicon-substitutional Cr or Ti atom. Under this assumption, two models for the V configuration have to be discussed: model *A*, the Si-substitutional site (labeled V_{Si}) is identical with V_4, model *B*, the Si-substitutional site V_{Si} is identical with V_{impl}.

In both cases, there is no experimental basis for any speculation about the defect structure of the other configurations. There is large number of possible candidates, including different sublattices, interstitial sites and complexing with intrinsic or other extrinsic defects.

Model *A* implies that most of the V atoms are involved in configurations different from V_{Si}. This means that both elemental transmutations involve a structural change in the majority of all decay events, either preventing the formation of V_{Si} out of a transmuting Cr_{Si} atom or creating Ti_{Si} out of a transmuting V_{impl} atom. These structural changes would require a sufficient mobility of defects at room temperature and cannot be explained completely by the decay-induced recoil because of the low recoil energy of the ^{51}Cr decay. Therefore, model *A* is unlikely.

Model *B* implies that V_{Si} does not have a band-gap state that would be detectable by the present DLTS measurements. On the other hand, an acceptor level of this configuration in the upper half of the band gap is clearly predicted from ESR work. To check the credibility of model *B*, one may try to find a level satisfying both conditions in the literature. First,

Jenny *et al.*[35] predict a vanadium state close to the conduction band. Such a state might be too shallow to be detected by DLTS. On the other hand, Evwaraye, Smith, and Mitchel[32] detect band-gap states in 4*H*-SiC at $E_C-0.87$ and -1.17 eV. Findings in the polytype 6*H* are similar[34] with levels detected at 0.78 and 1.09 eV. In the context of the present work, the level with smaller energy in both cases may be identified with site V_4 and the deeper level might be the acceptor level of V_{Si}. It is reasonable that such a level with an energy of 1.17 eV is not detected by the present DLTS measurements. This interpretation does not contradict reports of a V acceptor level around $E_C-0.70$ eV in 6*H*-SiC (Refs. 26 and 35) and around 0.8 eV in 4*H*-SiC (see Sec. IV E) since none of these measurements (resistance, DLTS) is sensitive to structure, i.e., they do not really prove that the observed level is due to V_{Si}. Instead, the results agree with level 4 (or its equivalent in 6*H*).

Model *B* may involve, but does not necessarily imply the occurrence of decay-induced defects in the present experiments, for the following reason: the creation of V_4 and $V_{daughter}$ during the ^{51}Cr decay is not necessarily a structural change of Cr_{Si} to these configurations. Instead, these atomic configurations might as well be formed initially by small, unobserved fractions of Cr atoms; their decay results in the corresponding structures of V without any need of a structural change. Because of the considerable errors of the electrical activation data [Fig. 8(a)], there may be enough Cr atoms left for such configurations. To explain the post-transmutation annealing experiments, one has to assume only that the configuration $V_{daughter}$ is generally unstable above 750 K whereas the same atomic configuration formed at a Cr atom is stable at the annealing temperature of 1600 K. Then, the relaxation effect observed is not really a decay-induced effect, but an instability of a daughter atom configuration (see Sec. II D). This scenario also explains the considerable scattering of the V_4 formation in the case of ^{51}V daughter atoms [Fig. 8(b)] since the concentration of V_4 is then determined by the relative population of the initial Cr configurations: in contrast to decay effects, this initial population may depend on implantation fluence, damage, or details of the annealing process and may thus vary from sample to sample. Remarkably, V_4 is populated during the ^{51}Cr decay exactly in those samples where it is present from the very beginning, i.e., formed by V atoms; this can be understood as a common trend to form this defect structure in these samples irrespective of the specific element.

Summarizing this discussion, model *A* implies unreasonable, but not principally impossible, decay-induced structural changes and is therefore improbable. Model *B* explains all results and does not contradict experimental findings in the literature; it states that the observed V acceptor level is not due to V_{Si}, but to some other unidentified configuration of V. The factors determining the relative population of the different V configurations and the transformations between them cannot be deduced from the present work.

VI. CONCLUSIONS

The band-gap states of Ti, V, and Cr in 4*H*-SiC carbide were characterized by DLTS on *n*-type 4*H*-SiC. A definite chemical identification is achieved by the elemental transmutation of radioactive isotopes. All band-gap states observed are definitely due to defects containing exactly one atom of the elements investigated. In the case of Ti and Cr, these defects are interpreted as a single impurity atom.

The results for each element studied will be summarized as follows. All energies refer to the conduction-band edge and are derived assuming a temperature-independent capture cross section.

Ti forms two slightly separated acceptor states close to the conduction-band edge of 4*H* SiC with energy levels at 0.127 (9) and 0.170 (9) eV, attributed to the inequivalent quasihexagonal and quasicubic lattice sites of 4*H*-SiC, respectively. These levels are formed both by directly implanted Ti atoms and—with a high efficiency of about 100%—by the Ti daughter atoms originating from the ^{48}V decay.

Cr forms three band-gap states in the part of the band gap investigated that are interpreted as two acceptor states of one Cr configuration. The double acceptor state close to the conduction band is slightly split into two levels at 0.143 (10) and 0.178 (10) eV. The single acceptor at 0.741 (15) eV is not split. Within errors (50%), these band-gap states are formed by all implanted Cr atoms.

In the case of vanadium, one band-gap state with at 0.97 (3) eV with an indication of splitting is detected. Despite some deviation concerning the energy, which is attributed to methodical reasons, this state is probably identical to the V acceptor state responsible for the compensating action of V in *n*-type SiC. This band-gap state, however, is formed by a minority of the implanted V atoms only. To explain this result, the atomic structure of the defects has been discussed, involving vanadium atoms in configurations different from the generally expected substitutional Si site. The best model assigns the observed V level to such a configuration and predicts the expected acceptor level of V_{Si} to be outside of the energy range investigated. Since V is incorporated in different configurations, their relative population and thus the electronic and optical properties of V-doped SiC are expected to depend on details of growth, doping, or annealing processes and not on concentration only.

Compared to V, the situation is rather simple for Ti and Cr, where the majority of all atoms forms the levels specified. Therefore, these band-gap states are unique fingerprints of the respective impurity atom and may be used in routine inspection or identification of impurities in SiC crystals.

ACKNOWLEDGMENTS

We thank J. Grillenberger and U. Reislöhner for assistance performing admittance spectroscopy, H. Hobert for performing Raman spectroscopy, and T. Licht and M. Rüb for assistance during the recoil implantation. Most important, we thank M. Frank and K. Rith (University Erlangen-Nürnberg) for providing and organizing beam time at the tandem accelerator of their institute. The work was funded by the German BMBF and by the Deutsche Forschungsgemeinschaft (DFG).

APPENDIX: QUANTITATIVE ANALYSIS OF INHOMOGENEOUS DEPTH PROFILES

In the standard treatment of DLTS, Poisson's equation is applied to the space charge region of a Schottky contact and

a general equation is derived[74] that links the band bending in this region to the concentration N_S and N_T of shallow and deep levels, respectively. Assuming $N_T \ll N_S$ and homogenous concentrations, the relative DLTS peak height finally reads

$$\frac{\Delta C}{C_R} = \frac{1}{2}\frac{N_T}{N_S}\frac{x_R^2 - x_P^2}{w_R^2}, \tag{A1}$$

where ΔC denotes the amplitude of the capacitance transient and C_R is the reverse bias capacitance. The geometrical quantities x and w are calculated from measured capacitances: w_R is the depth of the space charge region and the depths x_i ($i \in \{R,P\}$ for reverse bias or pulse conditions) denote the intersection between the trap energy and the Fermi level. The depth interval $[x_P;x_R]$ represents the part of the sample that contributes to the DLTS signal. Up to this point, all facts described reflect the standard evaluation of DLTS spectra.[50,51,75]

In the present work, traps with an inhomogenous depth distribution are to be investigated. Allowing the trap concentration to be a function $N_T(x)$, the resulting equation reads

$$\frac{\Delta C}{C_R} = \frac{1}{N_S}\frac{1}{w_R^2}\int_{x_P}^{x_R} x N_T(x)\,dx. \tag{A2}$$

For $N_T(x) = \text{const}$, Eq. (A2) reduces to Eq. (A1). For further evaluation, one has to assume some functional form of the profile shape, e.g., a two-parameter ansatz $N_T(x) = N_a f_s(x)$ with N_a being the integral over $N_T(x)$, i.e., the total number of traps per surface area and f_s being a normalized profile shape with a characteristic width s. Substituting this ansatz into Eq. (A2), all factors containing depth information can be summarized in a profile factor F_P as follows:

$$\frac{\Delta C}{C_R} = \frac{N_a}{N_S} F_P \quad \text{with} \quad F_P = \frac{1}{w_R^2}\int_{x_P}^{x_R} x f_s(x)\,dx. \tag{A3}$$

Except for the *a priori* unknown profile width s, all geometrical quantities entering Eq. (A3) can be calculated from experimentally measured capacitances. Regarding F_P as a function of s, it describes the sensitivity of certain measuring conditions to detect a certain trap distributed in depth according to $f_s(x)$. The dependence on trap parameters results from the temperature dependence of the capacitances and the Fermi-energy position.

In the present work, f_s is chosen to be a Gaussian profile centered at the surface, i.e., $f_s(x) = (2/\pi)^{1/2} s^{-1} \exp[-x^2/(2s^2)]$. Equation (A3) is used to determine the density N_a of traps per surface area from a given DLTS peak height ΔC. To judge the reliability of this procedure, the influence of the profile width s has to be discussed. Using individually calculated depth values w_R, x_P, and x_R, the profile factors of levels 1–6 are shown in Fig. 9(a) as a function of the profile width s. Qualitatively, the maximum of the profile factor occurs if the maximum of the integrand in Eq. (A3) lies within the sensitive interval $[x_P;x_R]$. The width parameters of all actually measured profiles [0.35–0.8 μm, Fig. 9(b)] are close to the maximum of the profile factor. Consequently, some uncertainty of the width parameter s does not result in large errors of the profile factor. The stability of this procedure essentially results from the proper choice of the depth scale, i.e., of the reverse bias and pulse voltages.

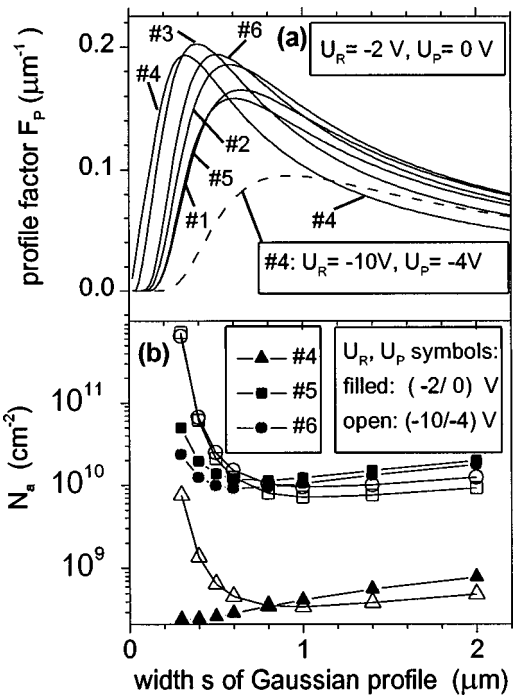

FIG. 9. (a) Profile factors F_P of the levels 1–6 as a function of the assumed profile width s. The solid lines reflect standard conditions. For level 4, the profile factor for greater measuring voltages is included additionally. (b) Number of traps per area which is necessary to explain the transmutation effects in sample 16 as a function of the assumed profile width s.

The profile factor can also be used to derive an estimate for the profile width if this quantity is unknown. For the sample show in Fig. 3 and both sets of measuring voltages used, the number of traps per area, N_a, is calculated from the observed peak height changes ΔC. Leaving the unknown profile width s as an independent variable, the result is shown in Fig. 9(b). It may be interpreted as the number of traps necessary to explain the observed peak height changes, if these traps are distributed in depth according $f_s(x)$. Clearly, different measuring voltages should give identical results. Thus, the intersection of the curves at around 0.8 μm for each of the three levels reveals that only this profile width is realistic and also directly yields the number of traps of each type actually present in the sample.

*FAX: ++49-3641-947302.
Electronic address: achtziger@pinet.uni-jena.de

[1] H. Morkoc, S. Strite, G. B. Gao, M. E. Lin, B. Sverdlov, and M. Burns, J. Appl. Phys. **76**, 1363 (1994).
[2] D. M. Brown, E. Downey, M. Ghezzo, J. Kretchmer, V. Krishnamurthy, W. Hennesy, and G. Michon, Solid-State Electron. **39**, 1531 (1996).
[3] G. Pensl and W. J. Choyke, Physica B **185**, 264 (1993).
[4] W. Wesch, Nucl. Instrum. Methods Phys. Res. B **116**, 305 (1996).

[5] G. Pensl and Th. Troffer, Solid State Phenom. **47 and 48**, 115 (1996).
[6] *Properties of Silicon Carbide*, edited by G. L. Harris, Emis Data Review Series No. 13 (INSPEC, London, 1995).
[7] N. Achtziger, J. Grillenberger, and W. Witthuhn, Appl. Phys. A: Mater. Sci. Process. **65**, 329 (1997).
[8] J. W. Petersen and J. Nielsen, Appl. Phys. Lett. **56**, 1122 (1990).
[9] M. Lang, G. Pensl, M. Gebhard, N. Achtziger, and M. Uhrmacher, Appl. Phys. A: Solids Surf. **53**, 94 (1991).
[10] A short review about radiotracer work in semiconductors can be found in N. Achtziger, Mater. Sci. Forum **248–249**, 113 (1997).
[11] N. Achtziger, T. Licht, U. Reislöhner, M. Rüb, and W. Witthuhn, in the *23rd International Conference on the Physics of Semiconductors*, edited by M. Scheffler and R. Zimmermann (World Scientific, Singapore, 1996), Vol. 4, pp. 2717–2720.
[12] N. Achtziger, J. Appl. Phys. **80**, 6286 (1996).
[13] A. Uddin, H. Mitsuhashi, and Tsutomo Uemoto, Jpn. J. Appl. Phys., Part 2 **33**, L908 (1994).
[14] H. McD. Hobgood, R. C. Glass, G. Augustine, R. H. Hopkins, J. Jenny, M. Skowronski, W. C. Mitchel, and M. Roth, Appl. Phys. Lett. **66**, 1364 (1995).
[15] St. G. Müller, D. Hofmann, A. Winnacker, E. N. Mokhov, and Yu. A. Vodakov, in *Silicon Carbide and Related Materials 1995*, edited by S. Nakashima, H. Matsunami, S. Yoshida, and H. Harima, Inst. Phys. Conf. Ser. **142** (Institute of Physics, London, 1996), p. 361.
[16] N. T. Son, E. Sörman, W. M. Chen, O. Kordina, B. Monemar, and E. Janzen, Appl. Phys. Lett. **65**, 2687 (1994).
[17] T. Kimoto, T. Nakajima, H. Matsunami, T. Nakata, and M. Inoue, Appl. Phys. Lett. **69**, 1113 (1996).
[18] J. Baur, M. Kunzer, and J. Schneider, Phys. Status Solidi A **162**, 153 (1997).
[19] J. Schneider and K. Maier, Physica B **185**, 199 (1993).
[20] K. Maier, H. D. Müller, and J. Schneider, Mater. Sci. Forum **83–87**, 1183 (1992).
[21] L. Patrik and W. J. Choyke, Phys. Rev. B **10**, 5091 (1974).
[22] K. M. Lee, Le Si Dang, G. D. Watkins, and W. J. Choyke, Phys. Rev. B **32**, 2273 (1985).
[23] T. Kimoto, H. Nishino, T. Ueda, A. Yamashita, W. S. Yoo, and H. Matsunami, Jpn. J. Appl. Phys., Part 2 **30**, L289 (1991).
[24] T. Dalibor, G. Pensl, N. Nordell, and A. Schöner, Phys. Rev. B **55**, 13 618 (1997).
[25] J. Schneider, H. D. Müller, K. Maier, W. Wilkening, F. Fuchs, A. Dörnen, S. Leibenzeder, and R. Stein, Appl. Phys. Lett. **56**, 1184 (1990).
[26] V. A. Il'in and V. A. Ballandovich, Defect Diffus. Forum **103–105**, 633 (1992).
[27] Th. Stiasny, R. Helbig, and R. A. Stein, in *Amorphous and Crystalline Silicon Carbide IV*, edited by C. Y. Yang, M. M. Rahman, and G. L. Harris, Springer Proceedings in Physics, Vol. 71 (Springer, Berlin, 1992), pp. 210–215.
[28] J. Reinke, H. Weihrich, S. Greulich-Weber, and J-M. Spaeth, Semicond. Sci. Technol. **8**, 1862 (1993).
[29] M. Kunzer, H. D. Müller, and U. Kaufmann, Phys. Rev. B **48**, 10 864 (1993).
[30] B. Kaufmann, A. Dörnen, and F. S. Ham, Mater. Sci. Forum **196–201**, 707 (1995).
[31] M. Kunzer, U. Kaufmann, K. Maier, and J. Schneider, Mater. Sci. Eng. B **29**, 118 (1995).
[32] A. O. Evwaraye, S. R. Smith, and W. C. Mitchel, Appl. Phys. Lett. **67**, 3319 (1995).
[33] J. R. Jenny, M. Skowronski, W. C. Mitchel, H. M. Hobgood, R. C. Glass, G. Augustine, and H. R. Hopkins, J. Appl. Phys. **78**, 3839 (1995).
[34] W. C. Mitchel, M. D. Roth, A. O. Evwaraye, P. W. Yu, S. R. Smith, J. Jenny, M. Skowronski, H. McD. Hobgood, R. C. Glass, G. Augustine, and R. H. Hoppkins (Ref. 15), p. 313.
[35] J. R. Jenny, J. Skowronski, W. C. Mitchel, H. M. Hobgood, R. C. Glass, G. Augustine, and H. R. Hopkins, Appl. Phys. Lett. **68**, 1963 (1996).
[36] A. O. Evwaraye, S. R. Smith, and W. C. Mitchel, J. Appl. Phys. **76**, 5769 (1994).
[37] P. G. Baranov, V. A. Khramtsov, and E. N. Mokhov, Semicond. Sci. Technol. **9**, 1340 (1994).
[38] N. Achtziger and W. Witthuhn, Mater. Sci. Eng. B **46**, 333 (1997).
[39] N. Achtziger and W. Witthuhn, Appl. Phys. Lett. **71**, 110 (1997).
[40] Assuming a capture cross section σ of 10^{-15} cm^2. Alternatively, the assumption of an extremely small σ of 10^{-19} cm^2 would reduce the upper limit to about 0.7 eV.
[41] N. Achtziger, H. Gottschalk, T. Licht, J. Meier, M. Rüb, U. Reislöhner, and W. Witthuhn, Appl. Phys. Lett. **66**, 2370 (1995).
[42] Samples implanted by nuclear reaction on a Ti foil contain the isotope ^{49}V. This isotope decays without γ emission to Ti with a half-life of 330 d. On the time scale of the present experiment, it is considered to be practically stable.
[43] S. Nakashima and H. Harima (Ref. 15), p. 269.
[44] L. Muehlhoff, W. J. Choyke, M. J. Bozak, and Joh. T. Yates, Jr., J. Appl. Phys. **60**, 2842 (1986).
[45] P. Blood and J. W. Orton, *The Electrical Characterization of Semiconductors: Majority Carriers and Electron States* (Academic, London, 1992), p. 492.
[46] J. L. Pautrat, B. Katircioglu, N. Magnea, D. Bensahel, J. C. Pfister, and L. Revoil, Solid-State Electron. **23**, 1159 (1980).
[47] W. Götz, A. Schöner, G. Pensl, W. Suttrop, W. J. Choyke, R. Stein, and S. Leibenzeder, J. Appl. Phys. **73**, 3332 (1993).
[48] A. O. Evwaraye, S. R. Smith, and W. C. Mitchel, J. Appl. Phys. **79**, 7726 (1996).
[49] D. V. Lang, J. Appl. Phys. **45**, 3023 (1974).
[50] P. Blood and J. W. Orton, *The Electrical Characterization of Semiconductor: Majority Carriers and Electron States* (Ref. 45), p. 344 and 426.
[51] J. Bourgoin and M. Lanoo, *Point Defects in Semiconductors II* (Springer, Berlin, 1983), p. 177.
[52] Model DL8020 from Biorad Inc. (Great Britain). The capacitance is measured with a 100 mV, 1 MHz test signal by a Boonton capacitance bridge and then digitized for further data processing.
[53] S. Weiss and R. Kassing, Solid-State Electron. **31**, 1733 (1988).
[54] Effective electron masses were taken from D. Volm, B. K. Meyer, D. M. Hofmann, W. M. Chen, N. T. Son, C. Persson, U. Lindefelt, O. Kordina, E. Sörman, A. O. Konstantinov, B. Monemar, and E. Janzén, Phys. Rev. B **53**, 15 409 (1996).
[55] V. N. Abakumov, V. I. Perel, and I. N. Yassievich, *Nonradiative Recombination in Semiconductors* (North-Holland, Amsterdam, 1991), p. 64.
[56] R. Sielemann, L. Wende, and G. Weyer, Phys. Rev. Lett. **75**, 1542 (1995).
[57] C. M. Lederer and V. S. Shirley, *Table of Isotopes* (Wiley, New York, 1978).
[58] R. B. Firestone and V. S. Shirley, *Table of Isotopes* (Wiley, New York, 1996).
[59] A. L. Barry, B. Lehmann, D. Fritsch, and D. Bräuning, IEEE

Trans. Nucl. Sci. **38**, 1111 (1991).
[60] J. Wong, T. Diaz de la Rubia, M. W. Guinan, M. Tobin, J. M. Perlado, A. S. Perez, and J. Sanz, J. Nucl. Mater. **212–215**, 143 (1994).
[61] DLTS spectra of sample 3 are shown in Ref. 39.
[62] M. Lang, G. Pensl, M. Gebhard, N. Achtziger, and M. Uhrmacher, Mater. Sci. Forum **83–87**, 1097 (1992).
[63] N. Achtziger and W. Witthuhn, Phys. Rev. Lett. **75**, 4484 (1995).
[64] A more detailed argumentation in a similar case is given in Ref. 12.
[65] This finding also implies that the removal and new preparation of contacts necessary for annealing above 850 K gives reproducible results.
[66] J. L. Hartke, J. Appl. Phys. **39**, 4871 (1968).
[67] T. Troffer, C. Peppermüller, G. Pensl, K. Rottner, and A. Schöner, J. Appl. Phys. **80**, 3739 (1996).
[68] The experimental limit for an eventual splitting of level 3 is 0.02 eV, assuming identical cross sections.
[69] J. M. Langer and H. Heinrich, Phys. Rev. Lett. **55**, 1414 (1985).
[70] N. Achtziger, J. Grillenberger, and W. Witthuhn, Mater. Sci. Forum **264-268**, 541 (1998).
[71] The assignment of an ESR signal to the Cr^{4+} state (Ref. 37) has since been corrected; see K. F. Dombrowski, M. Kunzer, U. Kaufmann, J. Schneider, P. G. Baranov, and E. N. Mokhov, Phys. Rev. B **54**, 7323 (1996).
[72] P. Käckell, B. Wenzien, and F. Bechstedt, Phys. Rev. B **50**, 10 761 (1994).
[73] M. Kunzer, thesis, University Freiburg, Germany, 1995.
[74] P. Blood and J. W. Orton, *The Electrical Characterization of Semiconductors: Majority Carriers and Electron States* (Ref. 45), p. 373, Eq. (7.50).
[75] G. L. Miller, D. V. Lang, and L. C. Kimmerling, Annu. Rev. Mater. Sci. **7**, 377 (1977).